2010 IEEE International Conference on Robotics and Automation
Anchorage Convention District
May 3-8, 2010, Anchorage, Alaska, USA

Design of an autonomous swimming miniature robot based on a novel concept of magnetic actuation

Giuseppe Tortora, *Student Member, IEEE*, Sebastiano Caccavaro, Pietro Valdastri, *Member, IEEE,* Arianna Menciassi, *Member, IEEE,* Paolo Dario, *Fellow, IEEE*

***Abstract*— In this work, we propose a new concept for locomotion of a miniature jellyfish-like robot based on the interaction of mobile permanent magnets. The robot is 35 mm in length and 15 mm in width, and it incorporates a rotary actuator, a magnetic rotor, several elastic magnetic tails and a polymeric body embedding a wireless microcontroller and power supply. The novel magnetic mechanism is very versatile for numerous applications and can be tailored and adapted on the basis of different specifications. An analytical model of the magnetic mechanism allows to shape the robot design based on the specific application. The working principle of the robot together with the design, prototyping and testing phases are illustrated in this paper.**

I. Introduction

Microrobotics is intended as the modeling, design and fabrication of robotic components and systems with size in the millimeter-micrometer range. Typical applications for microrobotic devices range from monitoring complex environments to medical applications [1], [2], [3]. A microrobot is an autonomous device that incorporates a control unit, a power source, and actuators for propulsion and steering. Microrobots have been proposed for many application environments, with flying [4], ground crawling [5] or swimming locomotion abilities [6].

In this work, we study the propulsion in fluids that is a fascinating and challenging topic where simple actuators and low forces can be used to achieve effective locomotion, as it happens for many small animals [7]. Due to the physics scaling laws, miniature robots swimming in fluids cannot be obtained by simply making traditional robots smaller, but must be based on radically different and novel concepts [8]. Several effective designs of small scale swimming robots have been proposed in literature.

Because of the very small Reynolds numbers at small scales (in the range of 1-2 mm), traditional principles of locomotion, as fins or propellers, cannot be efficiently applied. The Reynolds number, defined as the ratio of inertia to viscous forces, indicates that inertial components are negligible at the microscale. Since natural microorganisms have evolved in these conditions, a biomimetic approach holds the promise to achieve good performance in the most efficient way.

An example of swimming microrobot was discussed and modeled by Behkam and Sitti [9]. The propulsion concept is inspired by flagellar locomotion of bacteria. Another solution for the propulsion of a miniature swimming device was proposed by Kósa *et al*. [10]. The swimming action relies on the creation of a traveling wave along a piezoelectric layered beam divided into several segments. Such a robot paves the way to novel medical solutions in the fields of surgery, localized drug delivery, and therapy for vascular diseases.

By increasing the size up to 1-30 cm, other biomimetic devices were proposed for fluid environments, such as a tadpole swimming robot [11], a snake-like system [12], and several fish-like devices, electrostatic actuated [13], or flapping [14], or with sensing abilities [15]. Similar devices are used for swarm robotic applications, where an emergent behavior arose from a set of units which are implementing basic instructions [16]. A jellyfish-like robot, which relies on ionic polymer metal composite (IPMC) actuation, was also developed by Yeom and Oh [17]. Some devices have been proposed as autonomous underwater vehicles (AUVs), which have been extensively developed for a variety of applications ranging from environmental monitoring to oil and gas pipelines exploration [18]. However, these AUVs are not suitable for applications where the vehicle has to explore confined spaces or where maneuverability and stability are more important than speed, such as in medical applications. To achieve these goals, miniature-underwater vehicles (MUVs) should be very small, maneuverable, and precisely controllable.

In this work, we present a new concept for locomotion of a miniature jellyfish-like robot. This robot is based on a rotary actuator, a magnetic rotor, several elastic magnetic tails and a polymeric body integrating a wireless microcontroller and the power supply. The lateral tails are magnetically coupled with the internal rotating magnets, thus allowing the tails to flap and to propel the robot against the fluid.

This simple mechanism allows to achieve a wide range of performances by tailoring the design parameters in

Manuscript received on September 15, 2009. This material is based in part upon work supported by the Intelligent Microsystem Center, KIST, South Korea, and in part by the European Commission in the framework of the VECTOR FP6 European Project EU/IST-2006-033970.

All authors are with the Center of Research In Microengineering (CRIM) Laboratory, Scuola Superiore Sant'Anna, Pisa, Italy. A. M. and P. D. are also with the Italian Institute of Technology Network, Genova, Italy.

G. T. is the corresponding author (e-mail: g.tortora@crim.sssup.it).

order to meet the requirements of the specific application (e.g. miniature size, limited power consumption, high speed, tails activation gait, etc.). To this extent, the main objective of this work is to introduce the model and the design method of miniature jellyfish-like robots, rather than presenting a specific device, that can serve as an open platform for the development of innovative biomimetic miniature robots. Applications in the medical field, in environmental monitoring and in swarm robotics may be devised for this kind of autonomous robot.

II. Working Principle

A. Overview

The proposed device takes advantage of an innovative and simple concept for fluid-locomotion based on permanent magnets interaction. A set of magnets is mounted on a customized rotor driven by a motor, thus establishing a rotating magnetic field. A number of tails depart radially from the body of the robot. The tails, provided with a magnetized section, are moved by the interaction force with the rotating magnets. The resulting action enables locomotion in a liquid environment. The system can operate both "in repulsion", when a magnetic pole (either north or south) of the tail faces the same pole on the rotor, and "in attraction", when the magnetic pole of the tail faces the opposite pole on the rotor. Hybrid arrangements, mixing these configurations, are also possible depending on the devised application. A schematic representation of the working principle in repulsion configuration for one rotating magnet and four tails is shown in Fig. 1.

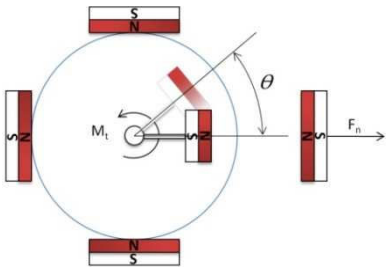

Fig. 1. Schematic representation of the working principle for a configuration "in repulsion" for one rotating magnet and four tails.

A 3D representation of the device is given in Fig. 2.The main modules of the proposed device are the tails, the rotating support of the magnet(s), the magnetic components, the internal actuator, and the body. Each module is featured by a series of possible variations which affect the design and the behavior of the whole system, as illustrated in this section. Afterwards, Section III discusses a possible robot implementation that has been designed by fixing some parameters for a preliminary feasibility study of the proposed locomotion concept.

1) Tails

The tails are elastic appendixes departing from the surface of the device acting on the liquid environment to generate thrust forces. They are hinged to the body and have a magnetized end which is actuated by the magnetic field generated by the internal rotating magnet(s). The tails can be manufactured in many shapes, sizes and materials. The number of tails can vary according to the different applications. The tail geometry and shape affect both the force and the interaction surface with the liquid. Therefore, the longer and wider the tail, the larger the action on the fluid is. The elastic properties of the tails must be considered in the design phase, because the structure stiffness influences the tail bending. The dependence of tail behavior on the design parameters is analyzed in subsection *C*. Composite materials embedding rigid structures in a polymeric matrix can be used to improve the tails performance (e.g. increasing the overall speed). In the following we refer to the "tail" as the assembly of the tail itself and the embedded magnets.

2) Rotating Support

In the robot body, a rotating support (the rotor) is connected to the motor shaft. One (as in Fig. 1) or more permanent magnets are housed inside the rotor with a specific direction of magnetization. The number of magnets depends on the desired behavior of the device. Once the direction of magnetization is fixed, if the number of magnets equals the number of tails, all tails bend simultaneously. Otherwise, the displacement of the tails can be set to perform asynchronized movements. The rotor diameter affects importantly the magnitude of the magnetic forces, by reducing or increasing the distance between the rotating magnetic field and the tails end. In the following, we refer to the "rotor" or "rotating support" as the assembly of the rotor itself and the magnet(s).

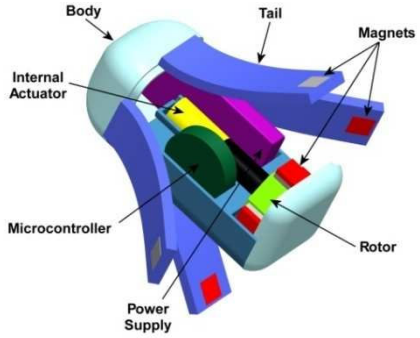

Fig. 2. 3D sketch of the device and its internal components.

3) Magnetic Components

Permanent magnets or magnetic microparticles dispersed in the tail structure can be used to obtain interaction between the tails and the rotor. Depending on the shape, the ratio between dimensions, the volume and the material grade, the magnetic behavior is different. In particular, NdFeB (Neodymium-Iron-Boron) magnets currently range in grade from N27 up to N52. The theoretical limit for NdFeB magnets is grade N64. Stronger magnets would increase tail bending, with the drawback of a higher torque required from the internal motor that generates the rotating magnetic field. On the other hand, small size magnets would allow miniaturization of the overall device, since a smaller internal actuator could be used. Also in this case, the final selection

must be based on the requirements of the specific application.

4) Internal Actuator

The embedded actuator has the function to generate a variable magnetic field by moving the permanent magnets mounted on board. The actuator must be featured by small dimensions, limited energy requirements and low weight. In addition, the actuator has to induce motion to the rotor embedding permanent magnets at different speed. In the current work we have considered commercial minimotors as internal actuators (see Section III), but Micro Electro-Mechanical Systems (MEMS) could be considered as internal actuators if we reduce the size of the entire device down to the millimeter.

5) Body

The external body must have a minimal volume to embed all the components of the device (rotating support, magnets, actuator, controller, telemetry, power supply), thus enabling applications at small scales. A drop-like body is the most convenient shape to keep the drag coefficient low, thus increasing locomotion performance. Rigid materials can be used to manufacture the shell in order to confer an adequate mechanical stiffness. Conversely, soft materials can be used as well for improving biomimetic features.

B. Analysis of Magnetic Forces

The interaction forces between two magnets depend on their volume, their geometry, the ratio between their characteristic dimensions, and the distance between them.

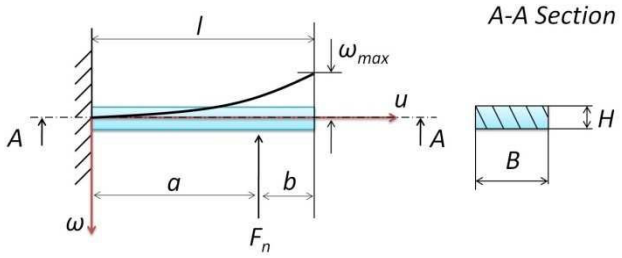

Fig. 3. Schematic of the cantilever beam. F_n, acting force; ω_{max}, stroke; l, beam length; a, distance between the point where the magnetic force is applied and hinge; b, l-a; B, tail width; H, tail thickness.

The force acting on an infinitesimal magnetic element (dV) is given by the Kelvin's formula:

$$\frac{\mathrm{d}\vec{\mathrm{F}}}{\mathrm{dV}} = \mu_0 \nabla(\vec{M} \cdot \vec{H}_{ext}), \tag{1}$$

where $\vec{M}$ is the magnetization and $\vec{H}_{ext}$ is the external magnetic field strength. Thus, the force acting on the whole magnet is obtained by integrating the differential force over the magnet volume V.

$$\vec{F} = \int_V \frac{\mathrm{d}\vec{\mathrm{F}}}{\mathrm{dV}} dV. \tag{2}$$

In order to calculate the magnetic force, the magnetic field $\vec{H}$ must be derived first. The distribution of $\vec{H}$ can be determined by using the method of the equivalent density current, as follows:

$$\vec{J}_m = \nabla \times \vec{M}, \tag{3}$$

$$\vec{K}_m = \vec{M} \times \hat{n}, \tag{4}$$

where $\vec{J}_m$ and $\vec{K}_m$ are the equivalent volume current densities in the material and on the surface, respectively, and $\hat{n}$ is the unit vector perpendicular to the surface.

We have applied the Biot-Savart law with the substitution of (3) and (4), and we have considered a direction of magnetization along the z axis, for a magnet having size $2w \times 2h \times 2t$ (along x, y, z axes respectively). The center of the magnet is the origin of the coordinates system and the magnetization M_0 is along z. Thus, the magnetic field is given by:

$$H_z = \left(\frac{M_0}{4\pi}\right)\left[\tan^{-1}\left(\frac{(x+w)(y+h)}{z\sqrt{(x+w)^2+(y+h)^2+z^2}}\right) + \tan^{-1}\left(\frac{(x-w)(y-h)}{z\sqrt{(x-w)^2+(y-h)^2+z^2}}\right) - \tan^{-1}\left(\frac{(x-w)(y+h)}{z\sqrt{(x-w)^2+(y+h)^2+z^2}}\right) - \tan^{-1}\left(\frac{(x+w)(y-h)}{z\sqrt{(x+w)^2+(y-h)^2+z^2}}\right)\right]. \tag{5}$$

By substituting (5) in (1) and integrating as in (2), the distribution of the force between the two magnets can be found. Obviously the obtained force is related to the magnet width w and height h, the ratio between them, and the relative position of the magnets [19]. The complexity of the equation increases with the number of interacting magnets, their shapes and relative position. Therefore, when multiple magnets are interacting, numerical or experimental solutions are usually preferred than a theoretical approach.

C. Cantilever Beam Model

A cantilever beam model has been adopted to analyze the tail bending. The schematics of the model and the considered parameters are illustrated in Fig. 3.

One end of the beam is hinged and a force F_n (that normally is the magnetic repulsion force in the selected configurations) acts at a distance a along the beam.

Using the Euler-Bernoulli model, the beam deflection (ω) can be described as:

$$\omega = \frac{-F_n u^2}{6EJ}(3a-u) \; for \; 0 < u < a, \tag{6}$$

$$\omega = \frac{-F_n a^2}{6EJ}(3u-a) \; for \; a < u < l, \tag{7}$$

where E is the Young's modulus of the material, J is the moment of inertia for the tail cross section BH, and l is the beam length. Considering the system working "in repulsion", F_n represents the radial component of the magnetic force F between one rotor magnet and the respective tail, and F_t is the tangential component. F_n produces the bending of the magnetic tail, whereas F_t generates the torque T_z that opposes to the movement of the

rotor. If F_n is known, the maximum deflection ω_{max} can be calculated. The bending distribution is an essential parameter in order to evaluate the hydrodynamic behavior of the tail, as reported in the following section.

D. Fluid dynamics

Optimizing the hydrodynamic behavior of the device is one of the main aspects for improving propulsion efficiency. A proper dimensioning of the tails affects the pressure generated by them on the fluid. The pressure p generated by a single tail can be calculated as following:

$$p = \frac{F_n}{A}, \tag{8}$$

where A is the active surface of the tail. By using (6) and (7), A is given by:

$$A = B\omega_{max}. \tag{9}$$

The parameter p can be used as reference for a comparative study on the system efficiency by varying number and shape of tails.

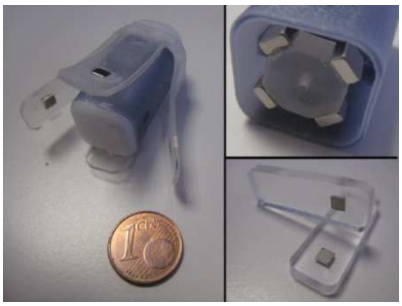

Fig. 4. Left: assembled prototype; up-right: detail of the rotor; bottom-right: detail of the tails.

III. Current Design and Prototyping

In the previous sections we have described the mechanism working principle and the dependence of the system performance on the different design parameters. Basically, the magnetic interaction force is related to the distance between the magnets, the tail stroke is influenced by its geometry and Young's modulus, whereas the tail shape affects the pressure generated by the robot onto the fluid. Although the proposed device is intrinsically simple, each module is characterized by many possible variations, thus leading to a virtually infinite set of possible configurations. In the current section, we validate the locomotion mechanism by fixing the design parameters in an average scale in order to obtain a working prototype with off-the-shelf and readily available components.

A. Technical Solution

A rotor embedding four magnets, a brushless motor and a battery are housed inside the body, whereas four tails are linked externally. The assembled prototype and a detail of rotor and tails are shown in Fig. 4.

Considering the size of the commercial available components to be integrated in the robot, we manufactured a rigid smooth-squared section shell 35 mm in length and 15 mm in width. This shape, regardless of hydrodynamic features, was considered suitable for allowing an easy assembling in preliminary experiments.

The rotor is an octagonal cross-section module designed to support four equally-spaced magnets. It has a diameter of 8.5 mm and a thickness of 4 mm. This is the maximum size available for a smooth integration in the shell by keeping maximum also the interaction force between internal magnets and tails.

Rapid prototyping (InvisionSi2 by Inition, ThingLab, London, UK) was employed for manufacturing both the shell and the rotor. The structural material is composed of urethane acrylate polymer (35-45%) and triethylene glycol dimethacrylate ester (45-55%).

Magnetic forces are generated by eight N42 NdFeB magnets (K&J Magnetics, Jamison, PA, USA), $3.18 \times 3.18 \times 1.59$ mm^3 in size and with a weight each of 0.120 g. Four permanent magnets are housed on the rotor with north pole facing outward, while the other four magnets are placed on the internal surface of the tails, in a repulsive configuration with the robot magnets. As the support rotates, the rotor magnets drive away the tail magnets periodically.

An SBL04-0829PG04-79 micromotor (Namiki, Akita, Japan) was selected as actuator for its small size and large torque (1.50 mNm), which is enough for driving the rotor, as illustrated in the next subsection. Such motor is 4 mm in diameter and 16.2 mm in length including the gearbox, and has a weight of 1.01 g.

A wireless microcontroller (μC) (CC2430, Texas Instruments, Dallas, TX, USA), mounted on a purposely developed circular electronic board (9.6 mm in diameter, 2.3 mm thick, 0.28 g of weight, [20]) was used to control the speed of the actuator remotely. It is also able to acquire data from sensors and to control additional actuators in case they will be embedded in future versions of the robot.

A Lithium Ion Polymer battery (LiPo) LP30 from Plantraco, having the highest energy density (200 Wh/kg) available for off-the-shelf components, was used to provide energy to all the active components of the robot. The LP30 is a 3.7 V LiPo cell with a nominal capacity of 30 mAh, a weight of 0.96 g, and very small size ($17 \times 10 \times 3$ mm^3).

Externally attached to the robot body, four elastic tails depart from the top of the device toward the bottom part. The tails, manufactured in polydimethylsiloxane (PDMS) material (Sylgard 184), are $30 \times 10 \times 1.7$ mm^3 in size. One end of the tail is hinged to the shell, while the opposite end embeds the NdFeB magnet and is free to move and bend. PDMS can be easily manufactured in different shapes and thickness, thus allowing to design and test many structural variations (e.g. with different elastic response and stroke). PDMS Young's modulus is 1.76 MPa [21].

1) Force Analysis

In this section, an analysis of the forces generated during the mechanism working is reported.

θ is the angle between one of the magnets placed on the rotor and a specific tail, as shown in Fig. 1. When $\theta = 0°$, all the rotor magnets face and repel the respective tails, thus achieving an unstable equilibrium position. If $\theta = 45°$, all the rotor magnets are symmetrically displaced respect to the tails, thus generating a stable equilibrium position.

Finite elements method (FEM) simulations were performed by COMSOL Multiphysics 3.5 to derive the force value F by means of its components F_n and F_t, and the torque T_z which opposes the motion of the rotor. The selected mesh consisted of 222068 elements, using a time-dependent system solver. Residual flux density (1.32 T) and relative permeability (1.05) were kept constant. The value of magnetization M_0 was $1.05 \cdot 10^6$ Am^{-1}.

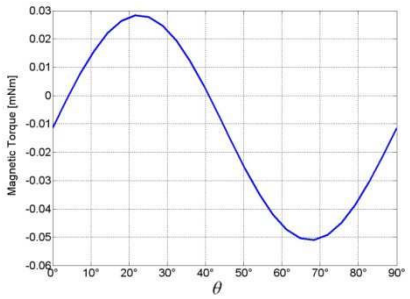

Fig. 5. Magnetic torque as function of θ (values derived from FEM analysis).

For an adequate dimensioning of the device, the most interesting values are represented by the maximum values of F_n and T_z. Fig. 5 shows that T_z is close to zero at θ = 0° (unstable equilibrium position), thus reaching the maximum value of 0.04 mNm at θ=22.5°, and going down to zero again at θ = 45° (stable equilibrium position). The value of $F_{n\,MAX}$, derived from FEM analysis, is about 0.04 mN.

This numerical solution agrees with the force value F_n calculated theoretically, thus validating the FEM model. In fact, Eq. (6) can be written as:

$$F_{n\,MAX} = -\frac{\omega_{u=a} EJ}{\left(\frac{au^2}{2} - \frac{u^3}{6}\right)} = -0.044\ N, \qquad (10)$$

being all parameters (ω, E, J, a) known for the given configuration of the device. $\omega_{u=a}$, measured empirically at θ = 0° in $u = a$, is 10 mm; E = 1.76 MPa, J = 6.66 mm^4; a = 20 mm.

B. Experimental Results

Experimental tests have been carried out in order to assess the locomotion performance and the behavior of the device.

The rotor speed can be wireless controlled by relating the index K with the commutation rate of the brushless motor (Table I). Since the electronics for controlling the motor is custom made, an evaluation of the motor parameters in working conditions must be done. The index K was related to the number of revolutions per minute (rpm) by considering the frequency of the motor without gearbox and by scaling it based on the gearbox reduction ratio.

The rpm was used to evaluate the theoretical number of beats for each tail, which is four times the rpm value, due to the presence of four magnets on the rotor. One beat begins when the tail starts bending and finishes when it comes back to the initial position. The theoretical number of beats per minute (bpm) matches the value measured in water, as seen in slow motion video capture, for K = 1 up to K = 8. If K > 8 one revolution of the rotor does not induce 4 beats anymore, since the mechanical response of the tails is not fast enough.

TABLE I
DYNAMIC BEHAVIOR OF THE ROBOT

K	Frequency (Hz)	Revolutions per Minute (rpm)	Beats per Minute (theoretical)	Beats per Minute (in water)
1	151.5	115	460	441
2	166.7	126	504	463
3	186.6	141	564	500
4	204.9	155	620	618
5	240.4	182	728	706
6	277.8	210	840	839
7	333.3	253	1012	1008
8	413.2	313	1252	1251
9	558.7	424	1696	787
10	625.0	474	1896	868

K, speed index; Frequency, referred to the motor before the gearbox; Revolution per Minute, referred to the speed of the rotor; Beats per Minute (theoretical), four times the rpm value; Beats per Minute (in water), observed in slow motion video.

Locomotion performance were tested in a liquid environment. The device was able to swim in water more than 15 minutes without recharging with a speed varying in a range between 0 and 3.7 cm/s, depending on the index K. An accompanying video showing locomotion performance is available.

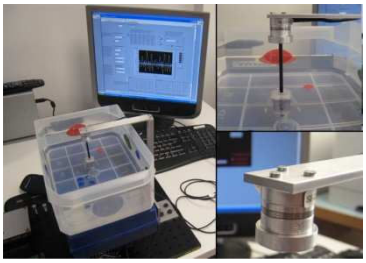

Fig. 6. Test bench for thrust measurements; up-right: detail of the support; bottom-right: detail of the load cell.

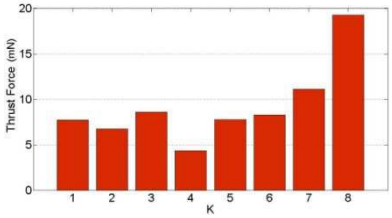

Fig. 7. Experimental values of thrust for different K values.

Force experiments were performed to quantify the effective forward thrust generated by the tails, by means of a commercially available 6-axis load cell (Nano17, ATI, Industrial Automation, Apex, NC, USA) having a resolution of 0.319 g. The robot was linked to the load cell through a rigid connection, thus allowing proper force transmission. The measuring system is shown in Fig. 6. After the robot

was fully submerged, the motor was activated for different K values. Fig. 7 reports the values of the thrust as a function of K; the thrust is almost constant for K between 1 and 6, thus increasing for K = 7, 8 because of the mechanical properties of the tails (i.e. for their elastic response). Values of K greater than 8 are missing because the PDMS appendixes were not sufficiently fast for generating thrust at high speed in water.

Power requirements were assessed for the presented prototype. The average current demand for the present configuration is about 100 mA when the motor is continuously working. When the motor is idle, the current demand goes down to about 0.5 μA, that is the average consumption of the μC.

C. Autonomous Control and Sensing

Since the proposed robot is mainly intended for the use as autonomous device, an advanced control must be implemented. Embedded sensors could provide the robot with environmental information, thus enabling variations of speed accordingly. A preliminary autonomous control was obtained by exploiting a temperature sensor integrated in the microcontroller, without additional components. Experiments showed that the robot can feel temperature variations of the liquid environment and can vary accordingly its speed. Different behaviors can be obtained if other sensors are integrated on board, depending on the devised application (e.g. pH, light, inertial or bio- sensors).

IV. Conclusions and Future Development

A new concept for locomotion of a miniature jellyfish-like robot was presented in this work. The working principle, the theoretical analysis, and the main robot modules were fully described. A preliminary prototype of the device was manufactured and tested. The prototype is composed of a micromotor, a magnetic rotor embedding 4 magnets, 4 elastic tails and a polymeric body holding a wireless microcontroller, a temperature sensor and the power supply. The device, tested in a fluid environment, was able to swim at a speed ranging between 0 and 3.70 cm/s, for more than 15 minutes. The working principle and the swimming capabilities are shown in the attached video.

This work aimed to introduce a general design method for the development of innovative miniature and simple biomimetic robots without addressing a specific application. On the other hand, the novel device is very versatile for applications in the medical field, in environmental monitoring and in swarm robotics. Future work will be carried on investigating different configurations of the robot and additional degrees of freedom (e.g. embedding smart and active materials into the tails).

References

[1] K. B. Yesin, K. Vollmers, and B. J. Nelson, "Modeling and control of untethered biomicrorobots in a fluidic environment using electromagnetic fields", *The International Journal of Robotics Research*, vol. 25, no. 5–6, pp. 527–536, May-June 2006.

[2] S.Guo, Q. Pan, and M. B. Khamesee, "Development of a novel type of microrobot for biomedical application", *Microsyst Technol*, vol. 14, no. 3, pp. 307–314, 2008.

[3] S. Martel, O. Felfoul, J.-B Mathieu, A. Chanu, S. Tamaz, M. Mohammadi, M. Mankiewicz, and N. Tabatabaei, "MRI-based medical nanorobotic platform for the control of magnetic nanoparticles and flagellated bacteria for target interventions in human capillaries", *The International Journal of Robotics Research*, vol. 28, no. 9, pp. 1169–1182, September 2009.

[4] R. J. Wood, The first takeoff of a biologically inspired at-scale robotic insect, *IEEE Transactions on Robotics*, vol. 24, no. 2, pp. 341–347, April 2008.

[5] B. Kim, M. G. Lee, Y. P. Lee, Y. Kim, G. Lee, "An earthworm-like micro robot using shape memory alloy actuator", *Sensors and Actuators A: Physical*, vol. 125, no. 2, pp. 429–437, January 2006.

[6] Z. Wang, G. Hang, J. Li, Y. Wang, and K. Xiao, "A micro-robot fish with embedded SMA wire actuated flexible biomimetic fin", *Sensors and Actuators A: Physical*, vol. 144, no. 2, pp. 354–360, June 2008.

[7] J. J. Abbott, K. E. Peyer, M. Cosentino Lagomarsino, L. Zhang, L. Dong, I. K. Kaliakatsos, and B. J. Nelson, "How should microrobots swim?", *The International Journal of Robotics Research*, vol. 25, no. 5–6, pp. 527–536, May-June 2006.

[8] J. J. Abbott, Z. Nagy, F. Beyeler, B. J. Nelson, "Robotics in the small, part I: microrobotics", *IEEE Robotics & Automation Magazine*, vol. 14, no. 2, 92–103, June 2007.

[9] B. Behkam and M. E. Sitti, "Modeling and testing of a biomimetic flagellar propulsion method for microscale biomedical swimming robots", in 2005 *Proc. of the IEEE/ASME International Conference on Advanced Intelligent Mechatronics*, pp. 37–42.

[10] G. Kósa, M. Shoham, and M. Zaaroor, "Propulsion method for swimming microrobots", *IEEE Transactions on Robotics*, vol. 23, no. 1, pp. 137–150, February 2007.

[11] B. Kim, D.-H. Kim, J. Jung, and J.-O. Park, "A biomimetic undulatory tadpole robot using ionic polymer–metal composite actuators", *Smart Material and Structure*, vol. 14, no. 6, pp. 1579–1585, November 2005.

[12] C. Stefanini, G. Orlandi, A. Menciassi, Y. Ravier, G. La Spina, S. Grillner, and P. Dario, "A mechanism for biomimetic actuation in lamprey-like robots", in 2006 *Proc. of the first IEEE/RAS-EMBS International Conference on Biomedical Robotics and Biomechatronics*, pp. 579–584.

[13] Z. G. Zhang, N. Yamashita, M. Gondo, A. Yamamoto, and T. Higuchi, Electrostatically Actuated Robotic Fish: Design and Control for High-Mobility Open-Loop Swimming, *IEEE Transactions on Robotics*, vol. 24, no. 1, pp. 118–129, February 2008.

[14] P. Kodati, J. Hinkle, A. Winn, and X. Deng, "Microautonomous robotic ostraciiform (MARCO): hydrodynamics, design, and fabrication", *IEEE Transactions on Robotics*, vol. 24, no. 1, pp. 570–578, February 2008.

[15] X. Tan, D. Kim, N. Usher, D. Laboy, J. Jackson, A. Kapetanovic, J. Rapai, B. Sabadus, and X. Zhou, "An autonomous robotic fish for mobile sensing", in 2006 *Proc. of the IEEE/RSJ International Conference on Intelligent Robots and Systems*, pp. 5424–5429.

[16] P. Valdastri, P. Corradi, A. Menciassi, T. Schmickl, K. Crailsheim, J. Seyfried, and P. Dario, "Micromanipulation, communication, swarm intelligence issues in a swarm microrobotic platform", "*Robotics and Autonomous Systems"*, vol 54, pp. 789–804, 2006.

[17] S.-W. Yeom and I.-K. Oh, "A biomimetic jellyfish robot based on ionic polymer metal composite actuators", *Smart Material and Structure*, vol. 14, no. 8, June 2009.

[18] J. Yuh, "Design and control of autonomous underwater robots: A survey", *Autonomous Robots*, vol. 8, no. 1, pp. 7–24, January 2000.

[19] J. S. Agashe and D. P. Arnold, "A study of scaling and geometry effects on the forces between cuboidal and cylindrical magnets using analytical force solutions", *J. Phys. D: Appl. Phys.*, vol. 41, no. 10, April 2008.

[20] E. Susilo, P. Valdastri, A. Menciassi, and P. Dario, "A miniaturized wireless control platform for robotic capsular endoscopy using advanced pseudokernel approach", *Sensors and Actuators A: Physical*, 2009, in press.

[21] F. Schneider, J. Draheim, R. Kamberger, and U. Wallrabe, "Process and material properties of polydimethylsiloxane (PDMS) for Optical MEMS", *Sensors and Actuators A: Physical*, vol. 151, no. 2, April 2009.